Inorganic Chemistry
Article

Inorg. Chem. **2010**, *49*, 1433–1438 **1433**
DOI: 10.1021/ic9016257

Structural Studies of Technetium−Zirconium Alloys by X-ray Diffraction, High-Resolution Electron Microscopy, and First-Principles Calculations

Frederic Poineau,*,† Thomas Hartmann,‡ Philippe F. Weck,† Eunja Kim,§ G. W. Chinthaka Silva,† Gordon D. Jarvinen,‖ and Kenneth R. Czerwinski†,‡

†*Department of Chemistry, University of Nevada Las Vegas, Las Vegas, Nevada 89154,* ‡*Harry Reid Center for Environmental Studies, University of Nevada Las Vegas, Las Vegas, Nevada 89154,* §*Department of Physics and Astronomy, University of Nevada Las Vegas, Las Vegas, Nevada 89154, and* ‖*G. T. Seaborg Institute, Los Alamos National Laboratory, Los Alamos, New Mexico 87545*

Received August 13, 2009

The structural properties of Tc−Zr binary alloys were investigated using combined experimental and computational approaches. The Tc_2Zr and Tc_6Zr samples were characterized by X-ray diffraction analysis, scanning electron microscopy, electron probe microanalysis, and transmission electron microscopy. Our XRD results show that Tc_6Zr crystallizes in the cubic α-Mn-type structure ($I\bar{4}3m$ space group) with a variable stoichiometry of $Tc_{6.25-x}Zr$ ($0 < x < 1.45$), and Tc_2Zr has a hexagonal crystal lattice with a $MgZn_2$-type structure ($P6_3/mmc$ space group). Rietveld analysis of the powder XRD patterns and density functional calculations of the "Tc_6Zr" phase show a linear increase of the lattice parameter when moving from $Tc_{6.25}Zr$ to $Tc_{4..80}Zr$ compositions, similar to previous observations in the Re−Zr system. This variation of the composition of "Tc_6Zr" is explained by the substitution of Zr for Tc atoms in the 2a site of the α-Mn-type structure. These results suggest that the width of the "Tc_6Zr" phase needs to be included when constructing the Tc−Zr phase diagram. The bonding character and stability of the various Tc−Zr phases were also investigated from first principles. Calculations indicate that valence and conduction bands near the Fermi level are dominated by electrons occupying the 4d orbital. In particular, the highest-lying molecular orbitals of the valence band of Tc_2Zr are composed of d−d σ bonds, oriented along the normal axis of the (110) plane and linking the Zr network to the Tc framework. Strong d−d bonds stabilizing the Tc framework in the hexagonal unit cell are also in the valence band. In the cubic structures of Tc−Zr phases, only Tc 4d orbitals are found to significantly contribute near the Fermi level.

Introduction

Technetium, element 43, occurs in only trace quantities in the earth's crust, mainly from the spontaneous fission of ^{238}U. Thirty-four radioactive isotopes of the element are known, with mass numbers ranging from 85 to 118. The most common isotope, ^{99}Tc ($t_{1/2} = 2.13 \times 10^5$ y), is present in large quantities in spent nuclear fuel, where it constitutes approximately 6% of the fission yield.[1] In the context of nuclear waste management, Tc presents a threat to the biosphere because it is quite stable and mobile in an oxidizing environment as the pertechnetate anion. Two approaches to reduce the potential hazard are being considered for Tc: transmutation of a metallic Tc target by neutron capture in a reactor to produce stable ruthenium and incorporation of Tc in a very stable disposal form (e.g., Tc alloys or oxide materials) placed in a geological repository.[2,3] Technetium−stainless-steel−Zr alloys have been recently studied as potential candidates for the immobilization of Tc-containing residues from the processing of used fuel from the EBR-II reactor.[4,5] More detailed knowledge of the synthesis and properties of Tc-containing alloys is needed to evaluate their use as disposal forms.

We report here on structural studies and theoretical calculations on some Tc−Zr alloys as part of a systematic investigation of the alloys of Tc with other high-yield fission product metals such as Zr, Mo, Ru, and Pd. Structural

*To whom correspondence should be addressed. E-mail: freder29@unlv.nevada.edu.

(1) Schwochau, K. *Technetium: Chemistry and Radiopharmaceutical Applications*; Wiley-VCH: Weinheim, Germany, 2000.
(2) Bonnerot, J. M.; Broudic, V.; Phelip, M.; Jegou, C.; Varaine, F.; Deschanels, X.; Arnoux, M. F.; Faugere, J. L. *J. Nucl. Radiochem. Sci.* **2005**, *6*, 287–290.
(3) Frank, S. M.; Keiser, D. D.; Marsden, K. C. Immobilization of Technetium in a Metallic Waste Form. *Global 2007: Advanced Nuclear Fuel Cycles and Systems Proceedings*, Boise, ID, 2007; American Nuclear Society: La Grange Park, IL, 2007; pp 1404−1411.
(4) Keiser, D. D.; Abraham, D. P.; Richardson, J. W. *J. Nucl. Mater.* **2000**, *277*, 333–338.
(5) Johnson, S. G.; Frank, S. M.; Noy, M.; Disanto, T.; Keiser, D. D. *Radioact. Waste Manage.* **2002**, *22*, 300–326.

Published on Web 01/19/2010

studies on Tc−Zr alloys are sparse, and only two phases, Tc_6Zr and Tc_2Zr, have been identified so far.[6,7] Isomorphous with its rhenium homologue, Tc_6Zr was found to crystallize in the α-Mn cubic structure type (*Struktur-Bericht* designation A12), with superconductive properties at low temperatures (Tc = 9.7 K).[6] Superconductivities of Tc−Zr alloys were further investigated by theoretical methods.[9] Previous studies of Tc_2Zr suggest that this phase crystallizes in the $MgZn_2$-type hexagonal structure (S*truktur-Bericht* designation C14). The M_2Zr−C14 phase has also been reported for M = Mn, Re, Ru, and Os.[10] Theoretical calculations on the ^{99}Tc quadruple moment in Tc_2Zr have been performed, but no experimental values were reported.[11] Unlike the Re and Mn homologs, no Tc−Zr phase diagram has been reported, and Tc_2Zr and Tc_6Zr are still not fully characterized. Recent calculations on Tc−Zr alloys show the potential stability of Tc−Zr alloys with the theoretical compositions Tc_2Zr, TcZr, $TcZr_2$, and $TcZr_4$, while no data were reported for Tc_6Zr.[12]

To gain a better understanding of the Tc−Zr system, it is important to obtain accurate structural information on its existing phases (Tc_6Zr, Tc_2Zr). In the present work, two Tc−Zr alloys with approximate compositions "Tc_6Zr" and "Tc_2Zr" were synthesized and characterized by X-ray diffraction (XRD), scanning electron microscopy (SEM), transmission electron microscopy (TEM), electron probe microanalysis (EPMA), and first-principles calculations. The SEM and EPMA analyses both confirm the presence of Tc_6Zr and Tc_2Zr in the sample; an additional phase, with composition $Tc_{4.58(27)}Zr$, was found in the Tc_2Zr sample. The atomic coordinates and structural parameters of $Tc_{6.25-x}Zr$ ($0 < x < 1.45$) and Tc_2Zr were determined from a Rietveld analysis of powder XRD patterns and further confirmed by first-principles calculations. The electronic structures, bonding characters, and stabilities of the various Tc−Zr phases were also investigated computationally.

Experimental and Computational Methods

Preparation. ***Caution!*** *The isotope ^{99}Tc is a weak beta emitter (E_{max} = 292 keV).* All manipulations were performed in a designed-for-radiochemistry laboratory using efficient HEPA-filtered fume hoods; a polycarbonate shield was used when manipulating the powder. The NH_4TcO_4 starting material was obtained from stocks at the Los Alamos National Laboratory originally purchased from the Oak Ridge Isotope Office and purified according to a method previously described.[13] Technetium metal was synthesized by hydrogen reduction of NH_4TcO_4 at 750 °C and characterized by XRD. Zirconium metal was purchased from Alfa-Aesar. Two Tc−Zr alloys were synthesized by mixing Tc and Zr powders in an agate mortar (sample A: Tc = 85.1 mg, Zr = 13.0 mg; sample B: Tc = 70.4 mg, Zr = 30.6 mg). The powder was transferred into a 3 mm die and pressed for 15 min at 600 MPa. Before arc melting, the stoichiometry of alloys was $Tc_{6.05}Zr$ (sample A) and $Tc_{2.11}Zr$ (sample B). The resulting pellets were arc-melted several times under an argon atmosphere; a mass loss (∼5 mg) occurred during the arc melting. The fused samples were placed into an alumina boat surrounded by a Zr foil, sintered at 1400 °C for 6 h under an Ar atmosphere, and cooled to room temperature.

Scanning Electron Microscopy, Electron Probe Microanalysis, and Transmission Electron Microscopy. For EPMA and SEM analysis, the alloys were embedded in a resin and polished to a mirrored finish (1 μm). The EPMA measurements were performed using a JEOL JXA 8900 R instrument. Technetium metal and Zr metal were used as quantification standards for the samples. The uncertainty of the EPMA measurements is 3%. SEM imaging was performed on a JEOL scanning electron microscope, model JSM-5610, equipped with secondary electron and backscattered electron detectors. The TEM samples were prepared by grinding the alloys in an ethanol solution in an agate mortar and dispersing one drop of the solution onto a 3-mm-diameter carbon film supported on a copper grid. Experimental details for TEM imaging are described elsewhere.[14]

X-Ray Powder Diffraction. The samples (∼10−20 mg) were mixed with a standard (Silicon SRM 640c) dispersed on a silicon disk, covered with Kapton foil, and placed in the instrument for measurement. The XRD patterns were obtained using a PANalytical X'Pert Pro instrument with Cu Kα emission and an X'elerator multiple Si-strip solid-state detector. The XRD patterns were quantified by Rietveld analysis using the Topas 3.0 software.[15]

First-Principles Calculations. First-principles all-electron scalar relativistic calculations of the total energies and optimized geometries were performed using the spin-polarized density functional theory (DFT).[16] The exchange correlation energy was calculated using the generalized gradient approximation (GGA) with the parametrization of Perdew and Wang (PW91).[17] Double numerical basis sets including polarization functions on all atoms (DNP) were used in the calculations. The DNP basis set corresponds to a double-ζ-quality basis set with d-type polarization functions added to atoms heavier than hydrogen. The DNP basis set is comparable to 6-31G** Gaussian basis sets[18] with a better accuracy for a similar basis set size. In the generation of the numerical basis sets, a global orbital cutoff of 5.3 Å was used. The energy tolerance in the self-consistent field calculations was set to 10^{-6} Hartree. Optimized geometries were obtained using the direct inversion in a subspace method with an energy convergence tolerance of 10^{-5} Hartree and a gradient convergence of 2×10^{-3} Hartree/Å. The unit cells used in our calculations contained 58 atoms for $Tc_{4.8}Zr$ and $Tc_{6.25}Zr$, and 12 atoms for Tc_2Zr. The Monkhorst−Pack special *k*-point scheme[19] was used for structural optimizations and electronic properties calculations with a $4 \times 4 \times 4$ mesh for $Tc_{6.25}Zr$ and $Tc_{4.8}Zr$, and a $5 \times 5 \times 4$ mesh for Tc_2Zr. In order to calculate the band structures, *k*-point paths along the X−R−M−G−R and G−A−H−K−G−M−L−H symmetry points[20] have been used to sample the Brillouin zone of the Tc_6Zr and Tc_4Zr structures and the Tc_2Zr structure, respectively. Total and projected densities of states were further calculated with a Gaussian broadening of 0.002 Hartree applied.

(6) Compton, V. B.; Corenzwit, E.; Maita, J. P.; Matthias, B. T.; Morin, F. J. *Phys. Rev.* **1961**, *123*, 1567–1568.
(7) Darby, J. B.; Lam, D. J.; Norton, L. J.; Downey, J. W. *J. Less-Common Met.* **1962**, *4*, 558–563.
(8) Giorgi, A. L.; Szklarz, E. G. *J. Less-Common Met.* **1970**, *22*, 246–248.
(9) Chatterjee, P. *Phys. Status Solidi B* **1984**, *124*, 773–779.
(10) Massalski, T. B. *Binary Alloy Phase Diagrams*; ASM. International: Metals Park, OH, 1992.
(11) Errico, L; Darriba, G.; Renteria, M.; Tang, Z.; Emmerich, H.; Cottenier, S. *Phys. Rev. B* **2008**, *77*, 195118/1–195118/5.
(12) (a) Curtarolo, S.; Morgan, D.; Ceder, G. *CALPHAD* **2005**, *29*, 163–211. (b) Curtarolo, S. *Coarse-Graining and Data Mining Approaches to the Prediction of Structures and Their Dynamics*, Ph. D. Dissertation, MIT, **2003**.
(13) Poineau, F.; Sattelberger, A. P.; Conradson, S. D.; Czerwinski, K. R. *Inorg. Chem.* **2008**, *47*, 1991–1999.
(14) Silva, G. W. C.; Poineau, F.; Ma, L.; Czerwinski, K. R. *Inorg. Chem.* **2008**, *47*, 11738–11744.
(15) *Topas V2.0.: Profile and Structure Analysis Software for Powder Diffraction Data. User Manual*; Bruker AXS: Karlsruhe, Germany (2000).
(16) (a) Delley, B. *J. Chem. Phys.* **1990**, *92*, 508–517. (b) Delley, B. *J. Chem. Phys.* **2000**, *113*, 7756−7764. DMol3 is available as part of Materials Studio.
(17) Wang, Y.; Perdew, J. P. *Phys. Rev. B* **1992**, *45*, 13244–13249.
(18) Hehre, W. J.; Radom, L.; Schleyer, P. R.; Pople, J. A. *Ab Initio Molecular Orbital Theory*; Wiley: New York, 1986.
(19) Monkhorst, H. J.; Pack, J. D. *Phys. Rev. B* **1976**, *13*, 5188–5192.
(20) Bradley, C. R.; Cracknell, A. P. *The Mathematical Theory of Symmetry in Solids*; Clarendon Press: Oxford, U. K., 1972.

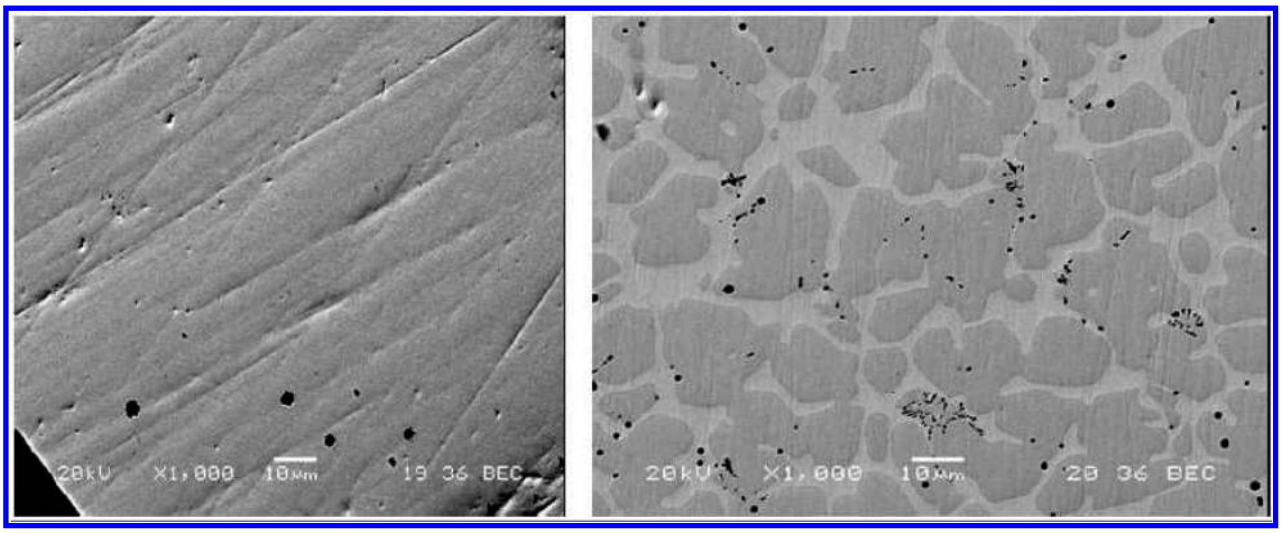

Figure 1. SEM images of sample A (left) and sample B (right) using backscattered electrons. The compositions (in atom %) determined by EPMA are Tc = 82.3% and Zr = 13.2% for sample A and Tc = 82.1% and Zr = 17.9% (light phase) and Tc = 64.4% and Zr = 31.5% (dark phase) for sample B.

Results and Discussion

Scanning Electron Microscopy. The SEM imaging indicates that sample A is monophase while sample B contains two phases (Figure 1). Further EPMA analysis confirms the composition $Tc_{6.24(37)}Zr$ for sample A, while for sample B, a $Tc_{2.04(12)}Zr$ stoichiometry is found for the dark phase and $Tc_{4.58(27)}Zr$ for the light phase. Several EPMA measurements performed on the phases in different regions of the samples indicate similar compositions. Nevertheless, the shift in the stoichiometry from $Tc_{6.05}Zr$ to $Tc_{6.24(37)}Zr$ for sample A and the presence of a phase with the composition $Tc_{4.58(27)}Zr$ in equilibrium with $Tc_{2.04(12)}Zr$ in sample B indicate a decrease of the Zr content during the synthesis. The loss of mass is attributed to the partial oxidation of Zr and the subsequent depletion of ZrO_2 from the alloy system during arc melting.

X-Ray Diffraction. Sample A contains $Tc_{6.25}Zr$ as the only phase, which crystallizes in the space group $I\bar{4}3m$. The crystal structure of $Tc_{6.25}Zr$ was refined on the basis of the structure description of α-Mn.[21] In the "Tc_6Zr" unit cell, the Zr atoms occupy the 8c positions, while Tc is expected to occupy two different 24g positions and one 2a position to account for the stoichiometry. The resulting stoichiometry is $Tc_{6.25}Zr$ if all positions (Wyckoff notation 2a, 8c, 24g, 24g) are fully occupied. This is obviously realized for the phase boundary with the highest Tc content, as found by EPMA analysis (i.e., $Tc_{6.24(37)}Zr$). The Tc_6Zr phase has a rather broad chemical stability field and reaches from $Tc_{6.25}Zr$ (highest Tc content) to $Tc_{4.8}Zr$ (lowest Tc content) and can be explained by the site occupancy of the 2a position. If the 2a position is fully occupied by Tc, a stoichiometry of $Tc_{6.25}Zr$ occurs. If the 2a position remains unoccupied, the phase stoichiometry is Tc_6Zr. Finally, if the 2a position is fully occupied by Zr, a $Tc_{4.8}Zr$ phase is observed. For the Tc_6Zr-type phase, the stoichiometries of the lowest Tc content (i.e., $Tc_{4.8}Zr$) and the highest Tc content (i.e., $Tc_{6.25}Zr$) deduced from XRD and site occupancy consideration are consistent with the results from EPMA (i.e., $Tc_{4.58(27)}Zr$ and $Tc_{6.24(37)}Zr$). For further clarity, these phases will be called $Tc_{4.8}Zr$ and $Tc_{6.25}Zr$. Using Rietveld structural refinement, the isotypy of $Tc_{6.25}Zr$ with α-Mn is confirmed, and the profile fit of the diffracted intensities provides low refinement residuals (Rwp) near 7.3%. The lattice parameter was refined to $a = 9.6104(2)$ Å.

Sample B contains the Laves phase Tc_2Zr, which crystallizes in the $MgZn_2$ structure type, and the "Tc_6Zr" type phase with the lowest Tc solubility ($Tc_{4.8}Zr$). Besides the "Tc_2Zr" and "$Tc_{4.8}Zr$" phases, the presence of a β-Zr phase ($Im\bar{3}m$, 0.1% in weight) as a nonequilibrium phase (lattice parameter $a = 3.223(4)$ Å) was found. Starting with the structure of $MgZn_2$, the Rietveld refinement of Tc_2Zr (Figure 2) was performed, and the atomic coordinates are presented in the Supporting Information. The lattice parameter of Tc_2Zr could be refined to high precision ($a = 5.2160(2)$ Å, $c = 8.6345(3)$ Å, unit cell volume $V = 203.4491$ Å^3), consistent with the published data of $V = 204.16$ Å^3.[7]

For the Tc_6Zr-type phase in sample B (i.e., $Tc_{4.8}Zr$), the lattice parameter found by Rietveld refinement (i.e., $a = 9.751(2)$ Å) is significantly larger than the one determined for the $Tc_{6.25}Zr$ phase in sample A (i.e., $a = 9.6104(2)$ Å). Isomorphic substitution of Tc by Zr in the 2a Wyckoff position of the α-Mn structure type has a strong impact on the unit cell dimensions. The lattice parameter of the "Tc_6Zr" phase enlarges by approximately 1 pm for every 10% substitution of Tc by Zr on the 2a position.

From the previous results, it is concluded that the stoichiometry of the Tc_6Zr-type phases can be explained by substitution of Tc atoms by Zr atoms at the 2a structural position to allow a rather broad phase stability field of $Tc_{6.25-x}Zr$ ($0 < x < 1.45$). The substitution accompanies an increase in the lattice parameter from 9.6104(2) Å for $x = 0$ to 9.751(2) Å for $x = 1.45$. In comparison, the value found by Darby et al. for $Tc_{6.0}Zr$ ($x = 0.25$) is 9.637(1) Å.[7] A similar behavior was observed in the Re−Zr system, where the phase $Re_{4.8}Zr$ (α-Mn) has a variable composition (80.6% Re and 82% Re) and a

(21) Kunitomi, N; Yamada, T.; Nakai, Y.; Fujii, Y. *J. Appl. Phys.* **1969**, *40*, 1265–1269.

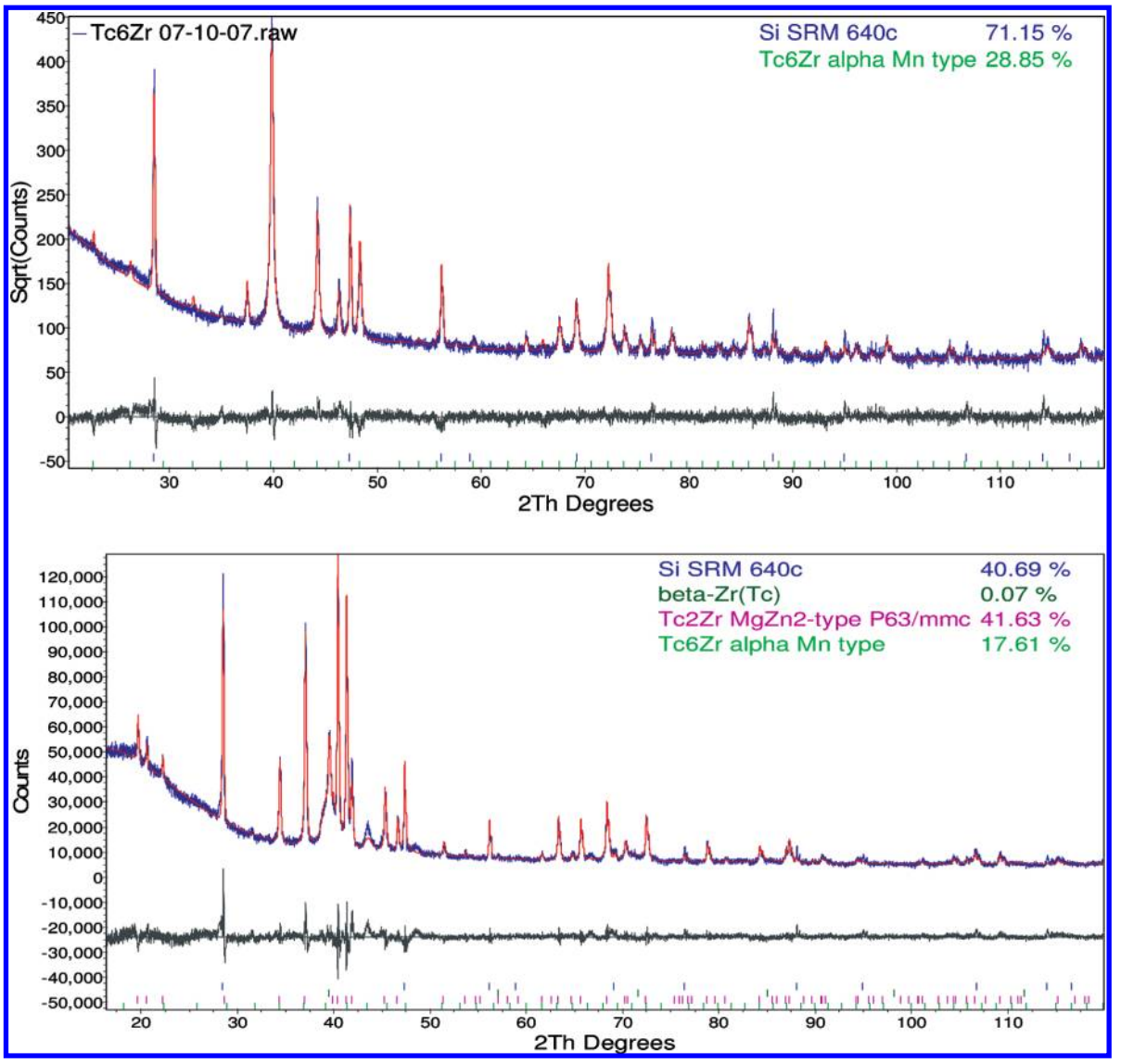

Figure 2. X-ray diffraction patterns of sample A (top) and sample B (bottom). In blue represents the experimental pattern, red the calculated pattern, and the gray at the bottom is the difference.

decrease of the lattice parameter is noted w (i.e., 9.626 and 9.693 Å, respectively).[22]

Transmission Electron Microscopy. The TEM analysis was performed on sample A in order to further investigate its crystallographic structure. HRTEM images (Figure 3a,b) and selected area electron diffraction (SAD) patterns (Figure 3c,d) were obtained at two different regions of the particle. The SAD patterns resemble the diffraction patterns of the α-Mn-type crystal structure in [101] and [100] zone axes, which confirm the crystallographic structure of the sample (see the X-Ray Diffraction section). The lattice fringes of the HRTEM and the corresponding FFT micrographs are also characteristic of the α-Mn structure type.

First-Principles Calculations. Both model $Tc_{6.25}Zr$ and $Tc_{4.8}Zr$ phases structurally relaxed with DFT have cubic crystal lattices with the α-Mn type and belong to the $I\bar{4}3m$ space group (Figure 4). The calculated lattice parameters for the relaxed cubic unit cells are $a = 9.99$ Å for $Tc_{4.8}Zr$ and $a = 9.93$ Å for $Tc_{6.25}Zr$, in fair agreement with the experimental values of $a = 9.7494$ Å and $a = 9.60989$ Å, respectively. This is consistent with the well-known fact that GGA functionals tend to overestimate bond lengths.

The model Tc_2Zr structure relaxed with DFT has a hexagonal crystal lattice with a $MgZn_2$-type structure (Figure 4) and belongs to the $P6_3/mmc$ space group. In Tc_2Zr, Zr occupies the 4f position of Mg, while Tc occupies all 2a and 6h positions of Zn. Lattice parameters for the relaxed hexagonal unit cell of Tc_2Zr are $a = 5.33$ Å and $c = 8.80$ Å ($c/a = 1.65$), compared to the experimental values of $a = 5.21611$ Å and $c = 8.63468$ Å ($c/a = 1.65539$). For all of the phases, the calculated interatomic distances (Table 1) show good agreement with X-ray diffraction data.

Figure 5 displays the band structure and the corresponding total and projected densities of states (DOS) of Tc_2Zr calculated using DFT. The band structures and DOS of $Tc_{4.8}Zr$ and $Tc_{6.25}Zr$ are presented as Supporting Information. All three compounds exhibit similar

(22) Savitskii, E. M.; Tylkina, M. A.; Tsyganova, I. A. *Sov. Atom. Energy* **1959**, *7*, 231–234.

characteristics, that is, a clear metallic behavior, with both valence and conduction bands dominated by 4d-orbital contributions from Tc and Zr atoms (Zr, [Kr]-$4d^2 5s^2$; Tc, [Kr]$4d^5 5s^2$), while s and p characters play only minor roles. Some degree of s−p and p−d hybridization appears in the valence and conduction bands. The calculated total electron densities of state at the Fermi surface are 72.3 and 85.6 states/eV for $Tc_{4.8}Zr$ and $Tc_{6.25}Zr$ (58 atoms/cell), respectively, and 12.5 states/eV for Tc_2Zr (12 atoms/cell). The high density of state near the Fermi level found for $Tc_{6.25}Zr$ is most likely due to the availability of a larger number of 4d electrons in Tc-rich alloys compared with Zr-rich systems, in a class of Tc−Zr alloys dominated by d-orbital character.

Figures 6 and 7 show the highest occupied molecular orbital (HOMO) of the Tc_2Zr, $Tc_{4.8}Zr$, and $Tc_{6.25}Zr$ structures. Consistent with the DOS shown above, the HOMO of all three structures is dominated by 4d orbitals.

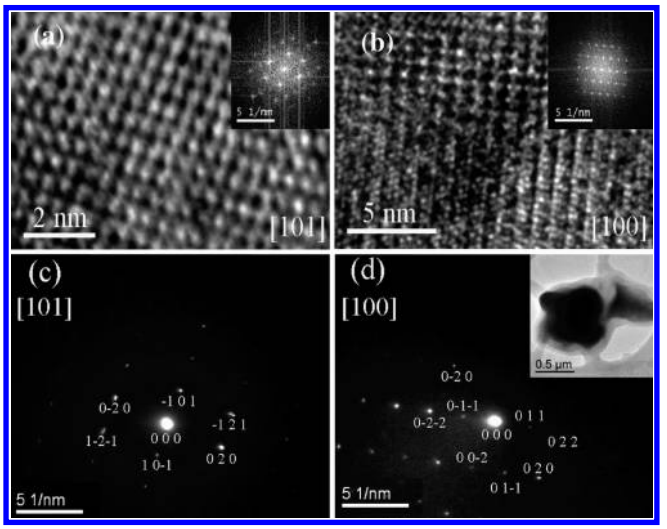

Figure 3. HRTEM images of sample A in different beam directions (bd) and SAD patterns in the same zone axes: (a) HRTEM image in [101] bd; (b) HRTEM in [100] bd; (c) SAD in [101] zone; (d) SAD in [100] zone. Insets in a and b are the FFT micrographs. The inset in d is the TEM BF of the particle used to obtain SAD patterns in c and d.

Table 1. Interatomic Distances from XRD Crystallographic Data and DFT Calculations for the Different Tc−Zr Phases

		distances (Å)	
phase	bonds	XRD	DFT
$Tc_{6.25}Zr$	Tc2−Tc3	2.532	2.60
	Tc3−Tc3	2.496, 2.603	2.58, 2.69
	Zr1−Tc2	2.756	2.86
	Tc−Zr1	3.019	3.13
$Tc_{4.8}Zr$	Tc2−Tc3	2.550	2.60
	Tc3−Tc3	2.529, 2.655	2.59, 2.72
	Zr1−Tc2	2.780	2.86
	Zr−Zr1	3.131	3.22
Tc_2Zr	Tc1−Tc2	2.653	2.70
	Tc2−Tc2	2.546	2.60
	Zr1−Zr1	3.214	3.27

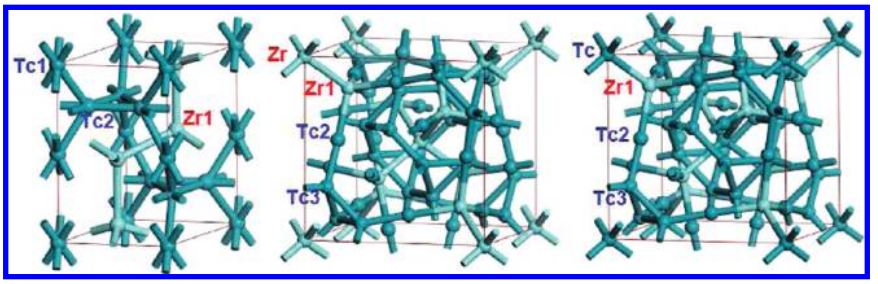

Figure 4. Stereographic view of the unit cells of Tc_2Zr (left), $Tc_{4.8}Zr$ (middle), and $Tc_{6.25}$ Zr (right).

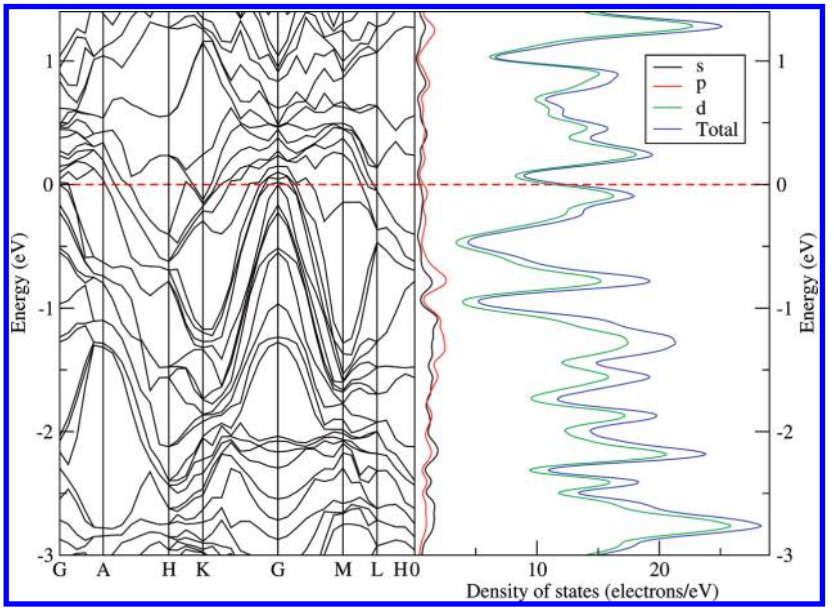

Figure 5. Band structure (left) and total and projected density of states of Tc_2Zr. The Fermi energy is set to zero.

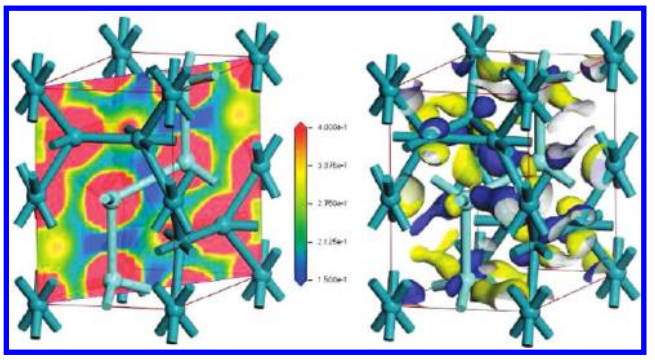

Figure 6. Electronic charge density projected onto the (110) plane (left; in units of $e/Å^3$) and highest occupied molecular orbital (right; fixed isovalue of 0.03 $e/Å^3$) of Tc_2Zr.

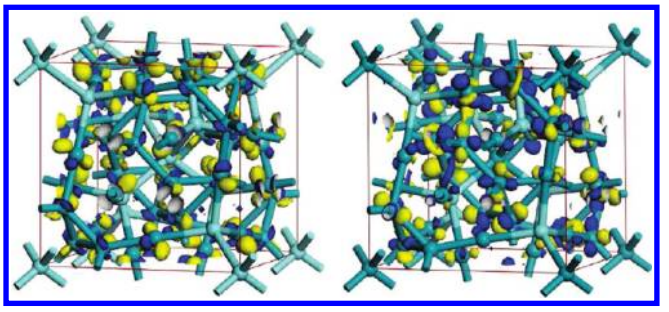

Figure 7. Highest occupied molecular orbital (fixed isovalue of 0.03$e/Å^3$) of $Tc_{4.8}Zr$ (left) and $Tc_{6.25}Zr$ (right).

Table 2. Atomic Charges Calculated Using DFT with Hirshfeld Partitioning of the Electron Density for the Various Phases of the Tc−Zr System

phase	atoms (charges in e)
Tc_2Zr	Zr1(+0.18), Tc1(−0.09), Tc2(−0.09)
$Tc_{4.8}Zr$	Zr(0.17), Zr1(0.17), Tc2(−0.01), Tc3(−0.06)
$Tc_{6.25}Zr$	Zr1 (+0.18), Tc2(−0.01), Tc3(−0.05), Tc(+0.03)

As shown in Figure 6, the HOMO of Tc_2Zr is composed of d−d σ bonds, oriented along the normal axis of the (110) plane and linking the Zr network to the Tc framework, as well as of d−d bonds stabilizing the Tc framework. This contrasts with the HOMO of the $Tc_{4.8}Zr$ and $Tc_{6.25}Zr$ phases where only Tc 4d orbitals contribute significantly (Figure 7). The projected electronic charge density for the Tc_2Zr cell displayed in Figure 6 shows a continuous electronic distribution along Tc1−Tc2 bonds, while the interactions between Tc1/Tc2 atoms and Zr atoms appear relatively limited in the (100) plane. Atomic charges calculated using the Hirshfeld partitioning of the electron density are presented in Table 2 for all of the phases. No significant variations of the atomic charges are observed for the different stoichiometries considered. The calculated charges are 0.17−0.18e on Zr atoms, while those determined for the Tc atoms vary slightly from −0.09e to +0.03e, depending on the local environment.

Conclusion

Technetium−zirconium alloys with approximate stoichiometry Tc_6Zr (sample A) and Tc_2Zr (sample B) were synthesized and structurally characterized. For sample A, a stoichiometry of $Tc_{6.25}Zr$ was found, and the lattice parameters and atomic coordinates were accurately refined. For sample B, results indicate equilibrium between Tc_2Zr and $Tc_{4.80}Zr$ phases. The XRD results on the Tc_2Zr phase are in good agreement with the literature, and atomic coordinates were successfully extracted. Concerning the phase $Tc_{4.80}Zr$, the XRD data indicate that it belongs to the α-Mn-type structure with a lattice parameter larger than $Tc_{6.25}Zr$. When results from samples A and B were combined, it was concluded that the "Tc_6Zr" phase has a variable composition, with stoichiometries ranging from $Tc_{6.25}Zr$ to $Tc_{4.80}Zr$. The lattice parameter increases when moving from $Tc_{6.25}Zr$ to $Tc_{4.80}Zr$. An analogous phenomenon has been observed in the Re−Zr system, where the lattice parameter of $Re_{25}Zr_4$ increases with the Zr content. This variation of the composition of the "Tc_6Zr" phase was explained by the substitution of Tc atoms by Zr in the 2a site in the α-Mn-type structure. These results indicate that the width of the "Tc_6Zr" phase needs to be included when constructing the Tc−Zr phase diagram.

The structural parameters experimentally found were successfully confirmed by first-principles calculations. The lattice parameter increase calculated by DFT when decreasing the Tc content from $Tc_{6.25}Zr$ to $Tc_{4.8}Zr$ was found to be in good agreement with the experimentally measured values. For all phases, electronic structure calculations indicate that valence and conduction bands near the Fermi level are dominated by the 4d orbitals. In particular, the highest-lying molecular orbitals of the valence band of Tc_2Zr are composed of d−d σ bonds, oriented along the normal axis of the (110) plane and linking the Zr network to the Tc framework, as well as of d−d bonds stabilizing the Tc framework. This contrasts with the $Tc_{4.8}Zr$ and $Tc_{6.25}Zr$ structures where only Tc 4d orbitals significantly contribute near the Fermi level. To further elucidate the Tc−Zr phase diagram, work on the synthesis and characterization of Tc−Zr (Zr > 50 atom %) is in progress, and results will be reported in due course.

Acknowledgment. The authors thank Mr. Tom O' Dou for health physics support. We also acknowledge Dr. Carol J. Burns (Los Alamos) for a generous loan of ammonium pertechnetate. Funding for this research was provided by a subcontract through Battelle 0089445 from the U.S. Department of Energy, agreement no. DE-AC07-05ID14517.

Supporting Information Available: Structural data from XRD crystallographic measurements, band structures, and densities of states of $Tc_{4.8}Zr$ and $Tc_{6.25}Zr$ calculated using DFT. This material is available free of charge via the Internet at http://pubs.acs.org.